lubricants

MDPI

Article

Comparative Study of Squalane Products as Sustainable Alternative to Polyalphaolefin: Oxidation Degradation Products and Impact on Physicochemical Properties

Jessica Pichler [1], Adam Agocs [1], Lucia Pisarova [1], Ichiro Minami [2], Marcella Frauscher [1] and Nicole Dörr [1,*]

[1] AC^{2}T research GmbH, Viktor-Kaplan-Str. 2/C, 2700 Wiener Neustadt, Austria; jessica.pichler@ac2t.at (J.P.); adam.agocs@ac2t.at (A.A.); lucia.pisarova@ac2t.at (L.P.); marcella.frauscher@ac2t.at (M.F.)
[2] Department of Engineering Sciences and Mathematics, Luleå University of Technology, 97187 Luleå, Sweden; ichiro.minami@ltu.se
* Correspondence: nicole.doerr@ac2t.at; Tel.: +43-(0)-2622-81600-150

Abstract: The growing demand for sustainable lubricant solutions is driving the exploration of bio-based materials that deliver comparable performance to conventional, primarily fossil-based lubricant chemistries. This study focuses on squalane as a sustainable base oil, which can be derived from different renewable sources. A total of two squalane products were evaluated for thermal-oxidative stability and benchmarked against a polyalphaolefin, PAO 4, of the same total carbon number. Oils artificially altered in a closed reactor were sampled and subjected to conventional lubricant analyses, including infrared spectroscopy, to determine the changes due to autoxidation over time. For in-depth information, direct-infusion high-resolution mass spectrometry and gas chromatography coupled with triple quadrupole mass spectrometry were employed to identify degradation products from thermo-oxidative stress. The results revealed substantial variability in the stability of squalane products, suggesting that differences in raw materials and production processes have a major impact on their performance, including rheological properties. The degradation products of polyalphaolefin and squalane, identified through detailed mass spectrometry, were analyzed to understand their impact on conventional physicochemical properties. While polyalphaolefin predominantly generated carboxylic acids with short to medium chain lengths as degradation products, squalane oxidation produced carboxylic acids with medium to long chain lengths as well as several alcohols and ketones. Despite these differences, squalane demonstrates its potential as a non-fossil hydrocarbon base oil, as squalane products matched and even exceeded PAO 4 stability.

Keywords: green lubricant; thermo-oxidative stability; sustainable lubricant; hydrocarbon-based lubricant base oil; squalane; polyalphaolefin

Received: 9 December 2024
Revised: 20 January 2025
Accepted: 21 January 2025
Published: 24 January 2025

Citation: Pichler, J.; Agocs, A.; Pisarova, L.; Minami, I.; Frauscher, M.; Dörr, N. Comparative Study of Squalane Products as Sustainable Alternative to Polyalphaolefin: Oxidation Degradation Products and Impact on Physicochemical Properties. *Lubricants* **2025**, *13*, 48. https://doi.org/10.3390/lubricants13020048

1. Introduction

Lubricants consist of a base oil blended with variable amounts of additives, the type and concentration of which depend on the specific application. Regarding relevance for sustainability, i.e., renewability, biodegradability, or recyclability, the base-oil component is the main critical consideration factor [1]. Nowadays, hydrocarbon-based polyalphaolefins (PAOs) are used as high-performing synthetic lubricant base oils thanks to their excellent properties, such as thermo-oxidative and hydrolytic stability, as well as their availability in a wide range of viscosity classes. Since they are commonly derived from petroleum or natural gas by the oligomerization of linear alphaolefins, they are not classified as renewable and

do not generally perform as "readily biodegradable" [2–4]. The lower viscosity of PAO 2 and PAO 4 make them the most easily biodegradable ones in aquatic environments, and although they are readily biodegradable, they have an inherent ability to undergo primary biodegradation [5,6].

There is a developmental shift toward lower-viscosity oils, especially in the automotive market. The new fuel economy targets low-viscosity grades as higher-viscosity lubricants tend to build fluid friction, contributing to a higher fuel consumption [7]. Development focuses on a viscosity of 5 W–30 (9–13 mm^2/s at 100 °C) down to a low viscosity of 0 W–20 (7–9 mm^2/s at 100 °C), and even to grades such as 0 W–16 (6–8 mm^2/s at 100 °C) [8,9]. For electric vehicles, synthetic PAOs or sustainable esters (1–7 mm^2/s at 100 °C) are in focus to provide higher efficiency in electric drive units. These oils should have pour points below −30 °C and neutralization numbers of less than 0.3 mg KOH/g oil [10,11]. Consequently, the use of high-performance additives is crucial to maintain consistent performance in lower-viscosity oils such as PAO 4 and squalane (~4 mm^2/s at 100 °C). The structure of PAO 4 is inherently branched with long sidechains, and it is a low-viscosity oil applied in demanding automotive and industrial lubricant applications [12]. Squalane prepared by the hydrogenation of squalene is more branched with methyl sidechains, shows good lubricating properties and is commonly used in the cosmetics industry as a skincare product [2,13].

A sustainable lubricant must minimize its environmental impact on soil, water, air, and biodiversity while guaranteeing a performance equal to or better than that of conventional fossil-based lubricants. Furthermore, to demonstrate renewability, bio-lubricants must contain minimum 25% bio-based carbon content in the final product in accordance with EN 16807 [14], as stipulated in the EU Ecolabel criteria [15]. The Ecolabel criteria were introduced to streamline the objective certification process for sustainable and environmentally benign lubricants. The related LuSC (Lubricant Substance Classification) list [16] was introduced to streamline the EU Ecolabel certification process for lubricants and provides a regularly updated inventory of lubricant components that comply with the Ecolabel criteria [17]. The strategy is that environmentally acceptable lubricants (EALs), such as those defined in the Vessel General Permit (VGP), replace non-sustainable, harmful mineral oils [18]. The first bio-based lubricant components that entered the market were made of triglycerides from vegetables [19]. These plant-based oils come with multiple benefits concerning their sustainability and biodegradability. Still, they also have the significant drawback of causing a food-chain conflict, directly using edible oils or indirectly using land for non-edible crop production [1,20]. There is a legislation push towards sustainable lubricant formulations that do not interfere with the food chain; for example, RED III (Renewable Energy Directive recast) highlights the need for a limited production of biofuels from cereal, starch-rich crops, oil crops, and sugar sources, referred to as advanced biofuels, to mitigate land-use change and its impacts. By 2020, a cap of a maximum of 7% of the total energy consumed in the transport sector in a Member State was applied for biofuels and bioliquids produced from food and feed crops, and it shall phase out via a gradual decrease to 0% by 2030. Additionally, the share of advanced biofuels in the transport sector shall surpass 5.5%, with at least 1% coming from Renewable Fuels of Non-Biological Origin (RFNBOs) by 2030, e.g., by using renewable electricity to convert carbon dioxide (CO_2) and water (H_2O) into hydrocarbons through chemical reactions like Fisher–Tropsch synthesis [21,22].

A seamless transition from non-bio-derived lubricants to more sustainable options is crucial for resource conversation and can be achieved by incorporating drop-in replacement components into existing formulations. The term "drop-in" originates in the field of fuels, referring to bio-derived materials blended into the conventional, mineral-based processing

pathway at an early stage, given their functional and chemical equivalence and using the benefit of well-established markets [23]. Bio-derived squalane has the potential to be a drop-in replacement component for low-viscosity synthetic PAO 4.

Squalane is a saturated, acyclic, branched C30 hydrocarbon—a more stable version of the naturally occurring unsaturated squalene. Squalene, a triterpene traditionally sourced from shark livers, can also be found in plant-based sources, including olives, amaranth seed, rice bran, palm, soy, or sunflower oil. Squalane can be processed from squalene hydrogenation, e.g., collecting it from acid oil, a processing residue (phytosqualane) from olive oil, or from the biotechnological process of fermentation with *Saccharomyces cerevisiae* into farnesene ($C_{15}H_{24}$) and carrying out its dimerization into squalene and hydrogenation to give saturated squalane [24,25].

Squalane was used previously as a model compound for the simulation of systems involving nonpolar lubricating oil with well-defined density and viscosity [26]. Recent studies include, e.g., polarity-dependent viscosity behavior combining experimental and computational methods [27]; the prediction of thermophysical properties (viscosity, density, self-diffusion coefficient) at extreme conditions of 1-decene trimer (such as PAO 4) and squalane using different force fields [28]; and elastohydrodynamic lubrication (EHL), comparing measured traction curves or using predictive simulation models in rolling/sliding tribometer rigs and discussing the complex rheological behavior of lubricants under extreme conditions [29–32].

To evaluate the stability of lubricant base oils and fully formulated lubricants, a large number of standardized methods are available, especially to determine the resistance against oxidation. Therefore, the sample is brought into contact with oxygen by passing gas through it, such as in the turbine oil oxidation stability test (TOST) prescribed in ASTM D943 [33], or in a closed reactor at elevated pressure, such as the rotary pressurized vessel oxidation test (RPVOT) described in ASTM D2272 [34]. Oxidation stability is assessed by the quantity of oxidation products (typically change in acidity and development of corrosiveness), oxygen absorption (pressure curve over time), viscosity changes, or the formation of sludge (weight of deposits or filtered residues), to name the most important parameters. However, advanced analytical methods are required to understand the degradation behavior of lubricants when exposed to oxygen to improve base-oil stabilities and predict the consequences on base-oil properties and performance. Gas chromatography coupled with mass spectroscopy (GC-MS) allows for the separation of complex mixtures such as lubricants and the identification of degradation products, e.g., [35]. While data on the oxidation stability of conventional base oils are well available from oil manufacturers, only a few known studies are about squalane. Besides the development of a kinetic model of squalane oxidation, GC-MS analyses revealed light hydrocarbons, alcohols, aldehydes, ketones, acids, and esters as degradation products [36]. The effect of biodiesel on the autoxidation of engine-oil base fluids was mimicked by a model system of methyl linoleate and squalane using GC-MS to determine the main degradation mechanisms [37].

This publication reports on a study on the characterization of squalane product streams for their usability as high-performing, well-defined, sustainable base oils benchmarked against the established synthetic PAO 4. For this purpose, artificial oil alteration was performed to examine the oxidative stability of both base-oil types and to determine the impact of raw materials and production processes on the performance and properties. In addition, major degradation products from artificially altered oil samples were identified using mass spectrometry techniques to understand their impact on the conventional physicochemical properties.

2. Materials and Methods

2.1. Base Oils

A selection of three squalanes (two from biotechnological origin and one from olive-oil waste processing) and one PAO 4 (derived from crude oil) was investigated. As shown in Figure 1 and discussed in Table 1, PAO 4 is mainly a 1-decene trimer that results from the oligomerization of a 1-decene alphaolefin and is then subjected to hydrogenation. Squalane is a natural structural isomer to PAO 4 with similar viscosity and a larger number of tertiary carbons due to a higher branching degree. Both structures have a sum formula of $C_{30}H_{62}$ and are composed of saturated hydrocarbon-based molecules imposing higher thermo-oxidative stability, leading to the suitability of PAO base oils for demanding high-temperature applications.

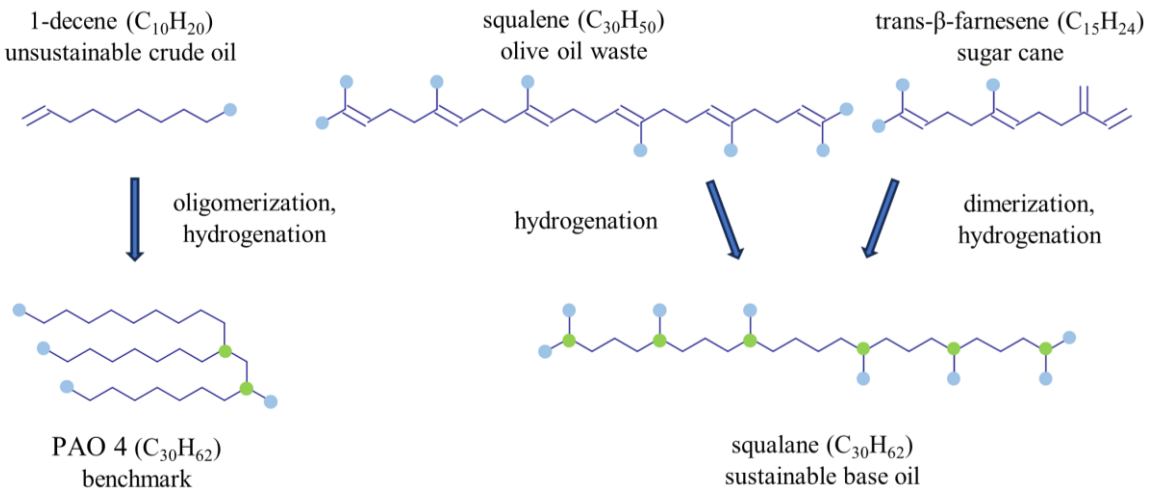

Figure 1. Main processing steps of $C_{30}H_{62}$ base oils sourced from different raw materials. Methyl groups are depicted by blue circles, and tertiary carbon atoms are marked with green circles.

Table 1. Overview of the selected base oils, including their feedstock, processing method, biodegradation, and renewability characteristics according to OECD 301B [38,39].

Sample ID	Origin	Processing Method	Biodegradability	Renewability
PAO 4	Crude oil, ethylene, 1-decene	Fully synthesized, distilled, and hydrogenated hydrocarbon base fluid produced from linear alpha olefin feedstocks [12]	Not ready	0%
Sugar-SQa	Sugarcane	Production of β-farnesene (precursor of squalene) through fermentation of sugar using the yeast *S. cerevisiae*, removal of yeast, hydrogenation, and purification to high-purity squalane [24]	Ready	100%
Sugar-SQb	Sugarcane	n.a.	Ready	100%
Olive-SQ	Olive-oil waste	Extracted as squalene from an unsaponifiable fraction of olive oil (acid oil) and hydrogenated to squalane [25]	Ready	100%

2.2. Oxidation Stability by Artificial Oil Alteration

To benchmark the selected squalanes against PAO 4, an accelerated simulation of thermo-oxidative degradation was conducted at the laboratory scale. This process, referred to as artificial alteration or artificial aging, is different from real-world aging in the application, where additional factors beyond constant temperature come into play. In this study, oxidation stability tests of the base oils were performed based on the method described in detail in [40]. This method is adapted from the rotary pressurized vessel oxidation test

(RPVOT) standard ASTM D2272-22 Method B [34], utilizing a TANNAS QUANTUM® Oxidation Tester (Tannas Co. & King Refrigeration Inc., Midland, MI, USA). The modified reaction cell and parameters enable clear differentiation between the samples and facilitate intermediate sampling. The magnetic cup assembly and sample beaker were replaced with a custom-made polytetrafluorethylene (PTFE) sample holder, which fits into the pressure chamber of the device with minimal dead volume. The sample is stirred with a magnetic stirrer to assist oxidation by utilizing the device's original drive and magnetic coupling. The sampling kit, also supplied by TANNAS, was further modified to reduce dead volume and to enable sampling even when the amount of liquid in the reaction cell is small.

A weighted base-oil sample was inserted into the PTFE sample holder and, subsequently, the pressure chamber. The system was closed and flushed with the reaction gas three times to remove all residual air, followed by setting the oxygen pressure to 2 bar above the atmospheric pressure. The pressure was monitored at room temperature for 15 min to verify the leak-proofness, then the reaction temperature was set by rapid heating to 120 °C. During the alteration procedure, small sample aliquots (approx. 1 g) were extracted via the sampling kit every hour starting from the second hour. Pressure and temperature were continuously monitored and recorded at a 5 s resolution. Table 2 summarizes the corresponding test parameters.

Table 2. RPVOT test parameters.

Parameter	Value
Temperature	120 °C
Reaction gas	Oxygen 5.0
Overpressure at start	2 bar
Sample amount	50 g
Stirring	100 rpm

Several standards utilize the monitored pressure decrease to determine oxidation stability, such as ASTM D2272 [34] and DIN EN 16091 [41]. Generally, once oxygen undergoes a chemical reaction with the oil sample, it ceases to exert pressure in the gas phase, resulting in a lower overall pressure recorded. Accordingly, the following related parameters were evaluated:

- Oxidation initiation time (OIT) corresponds to a 10% loss from the maximum pressure. This is analogous to the evaluation approach described in [41].
- Total oxidation time (TOT) describes the time until the pressure stabilizes at the end of the oxidation process. Within this work, this was defined as the overall change in pressure, namely the point where the pressure change is smaller than 0.25 mbar/min.

The alteration procedures were stopped at the TOT, and the reaction cell was cooled to room temperature to prevent further degradation reactions and to enable the recondensation of any volatiles formed. Subsequently, the final samples were collected and documented for analyses.

2.3. Conventional Lubricant Physicochemical Analyses

The determination and identification of oxidation degradation products by conventional (this chapter) and advanced (see Section 2.4) analytical methods require stable species. Therefore, oxidation stability was evaluated based on the analyses of alcohols, aldehydes, ketones, carboxylic acids, unsaturated compounds, and water.

Conventional physicochemical parameters of fresh, intermediate, and final oil samples were determined to generate a basic understanding of thermo-oxidative degradation evolution during artificial alteration. The following information was obtained

from a conventional characterization of the degree of degradation and its impact on physicochemical properties:

- Fourier-transform infrared (FT-IR) spectra of fresh, intermediate and final oil samples were recorded and compared to the fresh samples based on different spectra of transmission measurements with a liquid sample cell (ZnSe as window material, path length 100 µm) in a spectral (wavenumber) range of 4000–500 cm^{-1} (Tensor 27, Bruker Optik GmbH & Co. KG, Ettlingen, Germany):
  - Oxidation was determined by FT-IR using DIN 51453 [42] based on the peak height at 1710 cm^{-1} above a global baseline between 1970 and 580 cm^{-1}.
  - Unsaturation (unsaturated hydrocarbons) was established according to an in-house method determined based on the peak height at 1368 cm^{-1} above a global baseline extrapolated from 3900 and 2200 cm^{-1}.
- A neutralization number (NN) of the fresh and final oil samples (double determination) was acquired to account for the quantity of acids formed according to DIN 51558 [43] using titration with color indication with p-naphtholbenzein using a 0.05 M potassium hydroxide (≥85.0%, Supelco, Darmstadt, Germany) solution in 2-propanol.
- To identify water content, indirect Karl–Fisher (KF) titration was carried out via a heated gas flow moistened by water in the oil sample using a KF Coulometer and an Oven Sample Processor (Metrohm AG, Herisau, Switzerland) according to DIN 51777 [44] (double determination) for the fresh and final oil samples.
- The kinematic viscosity and density of the fresh and final oil samples were determined by an SVM 3000 Stabinger viscometer (Anton Paar GmbH, Graz, Austria). The applied method is based on ASTM D7042 [45], but the temperature range was extended from −40 °C to +100 °C to provide a better overview of the potential applicability. The viscosity index (VI) was calculated based on the kinematic viscosity data according to ASTM D2270 [46].
- The pour point (PP) according to DIN ISO 3016 [47] was determined for the fresh and altered oil samples using a mini pour point analyzer (PAC ISL MPP 5Gs, Houston, TX, USA).
- Simulated distillation was used for analyzing the boiling-range distribution of fresh and final altered oil samples by gas chromatography (GC) according to ASTM D6352 [48]. Briefly, 4% sample solutions in *n*-heptane were separated in a TG1MS (15 m × 0.25 mm × 0.25 µm, Thermo Fisher Scientific; Waltham, MA, USA) separation column starting at a temperature of 50 °C, followed by heating at 10 °C/min up to 300 °C and completed by holding this temperature for 30 min. During separation by GC, a helium flow of 10 mL/min was established, and eluted compounds were quantitatively determined with a flame ionization detector (FID). The boiling-range distribution was then calculated from the FID signal based on normalized retention time intervals.

Measurements with the Stabinger viscometer enable the comparison of changes in viscosity at low shear. The development of shear-dependent behavior, i.e., non-Newtonian behavior, cannot be excluded when these base oils are oxidized. Measurements over a wide shear range can reveal further differences between the base oils, enabling a comprehensive understanding of lubricant behavior and stability, but they were not in the scope of this study.

2.4. Advanced Chemical Analyses for In-Depth Characterization

2.4.1. Gas Chromatography Coupled with Mass Spectrometry (GC-MS)

Oil samples were examined by a Thermo Trace GC Ultra (Thermo Fisher, Bremen, Germany) gas chromatograph coupled in parallel to an FID and a Quantum XLS triple quadrupole mass spectrometer. Two different methods were conducted: boiling-range distribution by simulated distillation using GC-FID (see Section 2.3 last method) and the identification of degradation products by GC-MS (see the next paragraphs).

For compound identification, fresh, intermediate, and final oil samples were analyzed by GC-MS using a TG5MS fused silica column (30 m × 0.25 mm × 0.25 µm, Thermo Fisher Scientific; Waltham, MA, USA). Dichloromethane solvent (≥99.9%; Sigma-Aldrich, St. Louis, MO, USA) was used for sample dilution and N,O-Bis-(trimethylsilyl)trifluoroacetamide with trimethylchlorosilane (BSTFA + TMCS; 99%; Sigma-Aldrich, Buchs, Switzerland) was the derivatization agent.

The introduction of a trimethylsilyl (TMS) group to alcohols and organic acids facilitates separation by increasing volatility and identification through more expressive fragmentation patterns [49]. Therefore, samples were diluted to 4 wt% in dichloromethane, and BSTFA at 18 wt% was added as a silylation agent. The sample was silylated for one hour at 70 °C, and subsequently, 1 µL of the sample was injected at 300 °C with a 25:1 split ratio. Constant flow mode was used at 2 mL/min of helium carrier gas. The initial oven temperature was kept at 60 °C for 1 min, followed by a 10 °C/min ramp to 300 °C, and held for 25 min, resulting in a total run time of 50 min. The temperature of the transfer line from GC to MS was kept at 250 °C. The MS was equipped with an electron impact (EI) ionization source (70 eV) with a source temperature set to 200 °C, operated in a positive-ionization mode. Positive ions were generated by an electron emission current of 60 µA, and analytes were detected after a solvent cutoff time of 4.5 min within a mass-to-charge (m/z) range of m/z 40 to 650 and a scan time of 0.2 s. Data were acquired with Thermo Xcalibur 4.4.16.14 (Thermo Fisher) and evaluated with FreeStyle™ 1.8 SP2 (Thermo Fisher Scientific). The NIST20 mass spectral library (National Institute of Standards and Technology, U.S. Department of Commerce, Gaithersburg, MD, USA) was used to assist in compound identification. The adoption of compounds was based on a similarity search of mass spectra available in this database and mass spectra obtained in this study, as well as a plausibility check based on the initial chemical structures.

2.4.2. High-Resolution Mass Spectrometry (HR-MS)

The applied method is described in detail in [50] and briefly summarized below. The equipment used was an LTQ Orbitrap XL hybrid tandem high-resolution mass spectrometer (ThermoFisher Scientific, Bremen, Germany). Sample solutions were prepared in chloroform/methanol (7:3) (chloroform: ≥99.9%, Supelco, St. Louis, MO, USA; methanol: ≥99.9%; Supelco, Darmstadt, Germany) solvent with a dilution factor of 1:1000. The sample solutions were injected via automatized direct infusion into the IonMax API ion source, applying electrospray ionization (ESI) in positive- and negative-ionization modes and using nitrogen as the sheath gas. Fragmentation of the resulting single-charge ions was performed via low-energy collision-induced dissociation (CID) in the linear ion trap of the instrument using helium as both the buffer and collision gas. The resulting mass spectra were obtained within a range of m/z 50–800 by the high-resolution orbitrap mass analyzer (R = 30,000 FWHM at m/z 400).

Xcalibur version 2.0.7 and Mass Frontier version 6.0 software were used for the evaluation (both ThermoFisher Scientific, Bremen, Germany). The presented m/z refers to single-charged species. Hence, m/z is equivalent to the respective molecular mass. The

reported relative abundances are based on the total ion current (TIC) acquisition, where the highest ion signal in a mass spectrum corresponds to 100% of relative abundance.

3. Results and Discussion

3.1. Characterization of Fresh Oil Samples

Table 3 shows the summary of the determined conventional lubricant properties. All samples are characterized by very low and comparable acid levels (NN) as well as water contents, typical for neat (additive-free) hydrocarbons used as lubricant base oils. Olive-SQ has a higher pour point compared to all other base oils and a significantly higher viscosity at low temperatures.

Table 3. Comparison of fresh base oils by conventional lubricant parameters.

Oil Sample	PP (°C)	NN (mg KOH/g)	Water (ppm)	Kinematic Viscosity (mm^2/s)				VI (−)
				−20 °C	0 °C	40 °C	100 °C	
PAO 4	−75	<0.05	<10	407	106	17.5	4.0	128
Sugar-SQa	−72	<0.05	<20	687	142	19.0	4.1	117
Sugar-SQb	−72	<0.05	<20	689	142	19.1	4.1	115
Olive-SQ	−3	<0.05	<10	1798	204	22.2	4.5	116

Due to strong similarities of Sugar-SQa and Sugar-SQb in physicochemical properties and structural characterization, a reduction of the matrix was conducted, and degradation behavior was only studied for Sugar-SQa.

3.2. Thermo-Oxidative Stability and Conventional Oil Analyses

Figure 2a shows the FT-IR absorbance spectra of the fresh base oils. The wavenumber range from 3000 to 2800 cm^{-1} shows the presence of C-H groups (stretching) aligning with the vibrations around ~1450 cm^{-1} (scissoring), ~1380 cm^{-1} (methyl rocking), and ~730 cm^{-1} (rocking; long-chain alkanes), well visible in all base-oil types. The FT-IR difference spectra of the final altered samples are depicted in Figure 2b. Compared to the fresh base oils, the appearance of C=O carbonylic stretching vibrations in the range of 1670–1770 cm^{-1} is visible, indicating oxidation-derived carboxylic acids and ketones, and is in alignment with the neutralization number. Figure 2c,d illustrates enlarged views of the oxidation and unsaturation peaks together with the wavenumbers and baselines for peak height determination. Besides quantitative differences in peak height, the peak shapes suggest structural differences of C=O-containing compounds in altered PAOs and squalanes. The increase in the range of 3600–3150 cm^{-1} for O-H stretching refers to compounds containing the O-H group, typically water, alcohols and carboxylic acids. To find the main contributors to the O-H peaks, water content was evaluated from Karl–Fischer titrations, acidification levels expressed as NN were compared, and degradation products identified by GC-MS were viewed for alcohols (see Section 3.3.2). The most pronounced differences were found in the water contents and the detection of alcohols, both of which were higher for the squalane base oils than for PAO 4.

The trend of degradation product buildup is shown in Figures S1–S3 for PAO 4, Sugar-SQa, and Olive-SQ, respectively, taken from the intermediate and final oil samples and their FT-IR difference spectra compared to the fresh oil spectra.

Figure 3a illustrates the pressure curves of the three base oils. Sugar-SQa showed a similar TOT to the PAO 4. However, the total decrease in pressure was more pronounced in the case of Sugar-SQa. Comparatively, Olive-SQ displayed superior oxidation stability, characterized by a long initial phase of relatively constant pressure, whereas PAO 4 and Sugar-SQa already suffered considerable oxidation, and a slow decrease in pressure resulted

in a total alteration duration of 38 h compared to about 8.5 h in the case of PAO 4 and Sugar-SQa. As the sampling intervals were kept consistent during the alterations of the three base oils, the sampling of Olive-SQ was not optimal due to the unexpectedly slow oxidation progress.

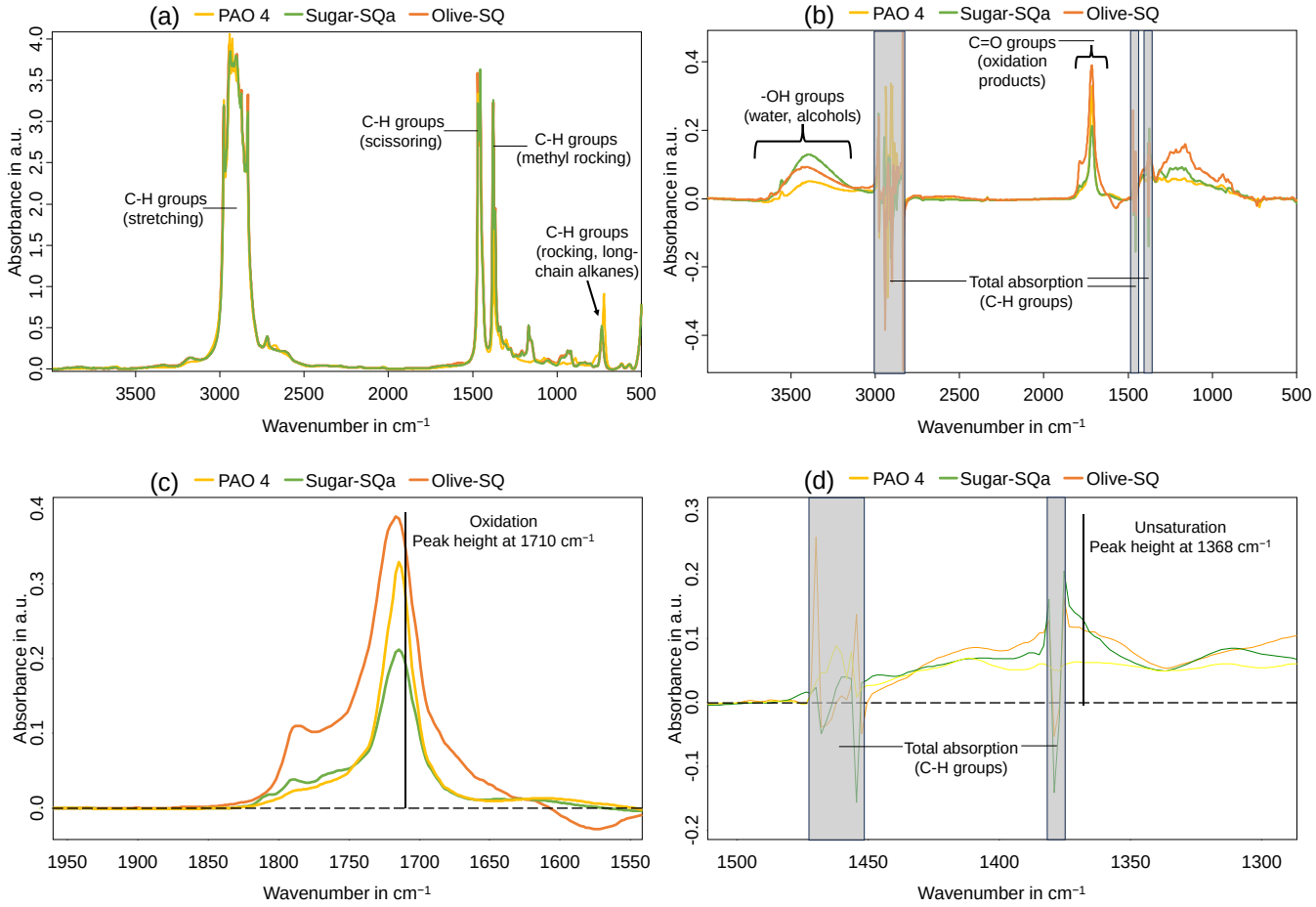

Figure 2. (**a**) FT-IR absorbance spectra of fresh base oils, (**b**) FT-IR difference spectra of final altered base oils, (**c**) Detail spectra for oxidation enlarged from (**b**), (**d**) Detail spectra for unsaturation enlarged from (**b**). In (**c**,**d**), vertical lines indicate the wavenumbers and horizontal lines the baselines for peak height determination.

The progress of oxidation corresponding to C=O bonds and unsaturation based on the obtained FT-IR spectra are displayed in Figure 3b,c for Sugar-SQa and PAO 4, respectively. The oxidation of hydrocarbons generally yields alcohols, aldehydes, ketones, carboxylic acids, ethers, esters, unsaturated hydrocarbons, carbon dioxide, and water through various radical reactions. PAO 4 base oil is characterized by a higher abundance of oxygen-containing products than Sugar-SQa, despite the lower pressure decrease, i.e., lower oxygen consumption. At first glance, this seems contradictory but can be explained by the different abundance of unsaturated hydrocarbons in Figure 3c, which is higher in Sugar-SQa compared to PAO 4. The wavenumber selected for evaluation represents isobutene and polyisobutenes, i.e., tertiary unsaturated carbon atoms. The bond dissociation energy (BDE) for carbon-hydrogen is in the order of C(tertiary)-H < C(secondary)-H < C(primary)-H. Therefore, tertiary carbons are more prone to hydrogen release compared to secondary and primary carbons; hence, they are more prone to form free radicals that initiate the autoxidation process [51,52]. Consequently, beta-hydrogen elimination from a tertiary-carbon radical takes place, which yields an alkene and dihydrogen. Also, beta-elimination from an alcohol formed by the oxidation of tertiary carbon results in the formation of

an alkene (double bond) and water. Obviously, in the case of Sugar-SQa, this reaction pathway is also prominent, leading to oxygen-containing species, at least compared to PAO 4. This interpretation is supported by the fact that squalane generally contains more tertiary carbons than PAOs (Figure 1).

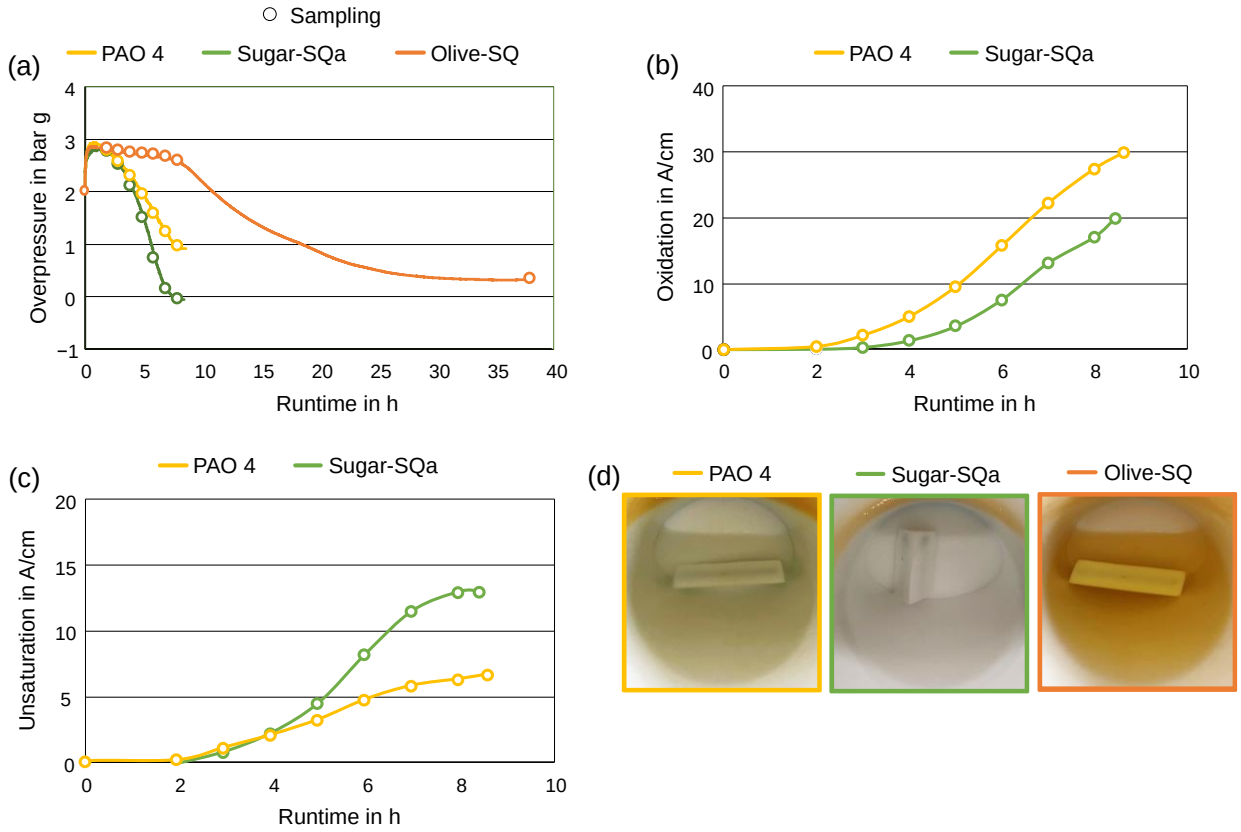

Figure 3. (**a**) Pressure curves of the base oils, (**b**) Oxidation during the artificial alterations (Sugar-SQa and PAO 4 only), (**c**) Unsaturated hydrocarbons during the artificial alteration (Sugar-SQa and PAO 4 only) (**d**) Photographic documentation at the end of the artificial alterations.

Since the intermediary samples of Olive-SQ were taken at an early stage with low oxygen pressure loss, no pronounced oxidation or accumulation of unsaturated hydrocarbons were detected. Consequently, the properties of Olive-SQ samples are not displayed in Figure 3b,c (see Figure 4 for the comparison to the final oil samples). Figure 3d displays the photographic documentation of the final oil samples at the end of the alteration procedures, still in the reaction cell. Sugar-SQa and PAO 4 show only minimal discoloration and are clear, whereas Olive-SQ has developed pronounced yellow color. None of the final oil samples contained sludge or deposit. The findings regarding pressure decline, oxidation, unsaturation, and discoloration demonstrate that PAOs and squalanes form different degradation products during oxidation.

Figure 4 provides an overview of the oxidation stability results and the relevant parameters determined in the final oil samples. All fresh samples were characterized by a negligible NN and water content (see Table 3). As mentioned, Sugar-SQa and PAO 4 exhibit similar oxidation stability, while Olive-SQ greatly exceeds those base-oil samples in OIT and TOT (see Figure 4a). Figure 4b shows the total pressure loss during the oxidation stability tests. The two squalane samples display a similar pressure loss, while PAO 4 seems to consume less oxygen in general. Oxidation and NN are displayed in Figure 4c,d. Here, NN is a measure for organic acids as typical oxidation products [53]. Accordingly, there is a clear correlation between the two parameters. Sugar-SQa shows the lowest oxidation and

NN in the final sample, while both parameters are higher in PAO 4 and even more elevated in Olive-SQ. Levels of unsaturated hydrocarbons and water are shown in Figure 4e,f. As discussed earlier, the variation of these parameters might be related to the number of tertiary carbon atoms. The final samples of the oxidation stability tests show a correlation between these two parameters: unsaturated hydrocarbons are more abundant in the final Sugar-SQa and Olive-SQ samples, and the water content is about twice as high compared to PAO 4. These findings suggest that squalanes are more susceptible to the degradation mechanism leading to unsaturation than polyalphaolefins.

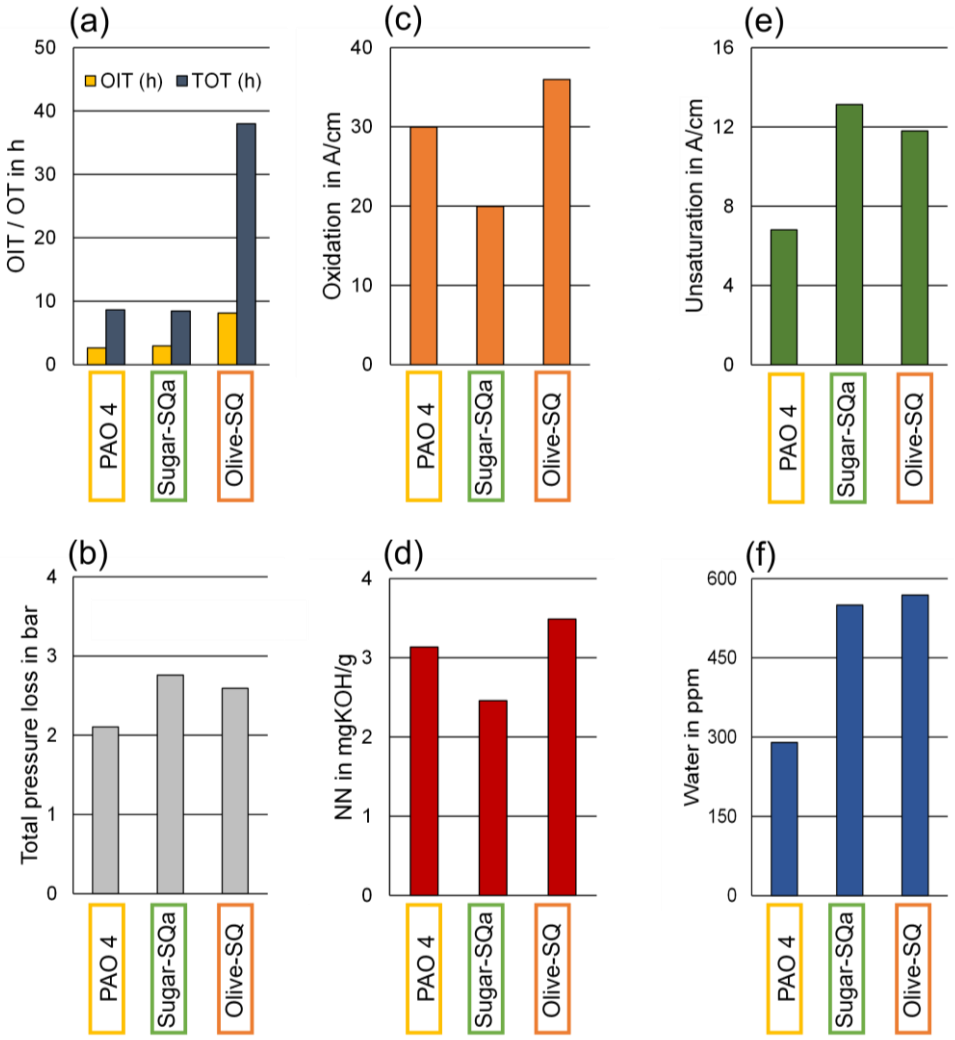

Figure 4. Characterization of the final oil samples: (**a**) OIT and TOT, (**b**) Total pressure loss, (**c**) Oxidation, (**d**) Neutralization number, (**e**) Unsaturation (unsaturated hydrocarbons), (**f**) Water content.

Figure 5 provides an overview of kinematic viscosity and density changes over a temperature range from −40 °C to +100 °C. The low- and high-temperature data are presented in separate figures to account for very high viscosities measured close to −40 °C. PAO 4 in Figure 5a,b generally shows comparable viscosity and density before and after artificial alteration (except below −30 °C). Apart from a slight increase in density and viscosity at low temperatures, degradation does not seem to affect these properties significantly. The measurement of the PAO 4 altered sample at −40 °C was not possible because the value was outside of the measuring range of the instrument.

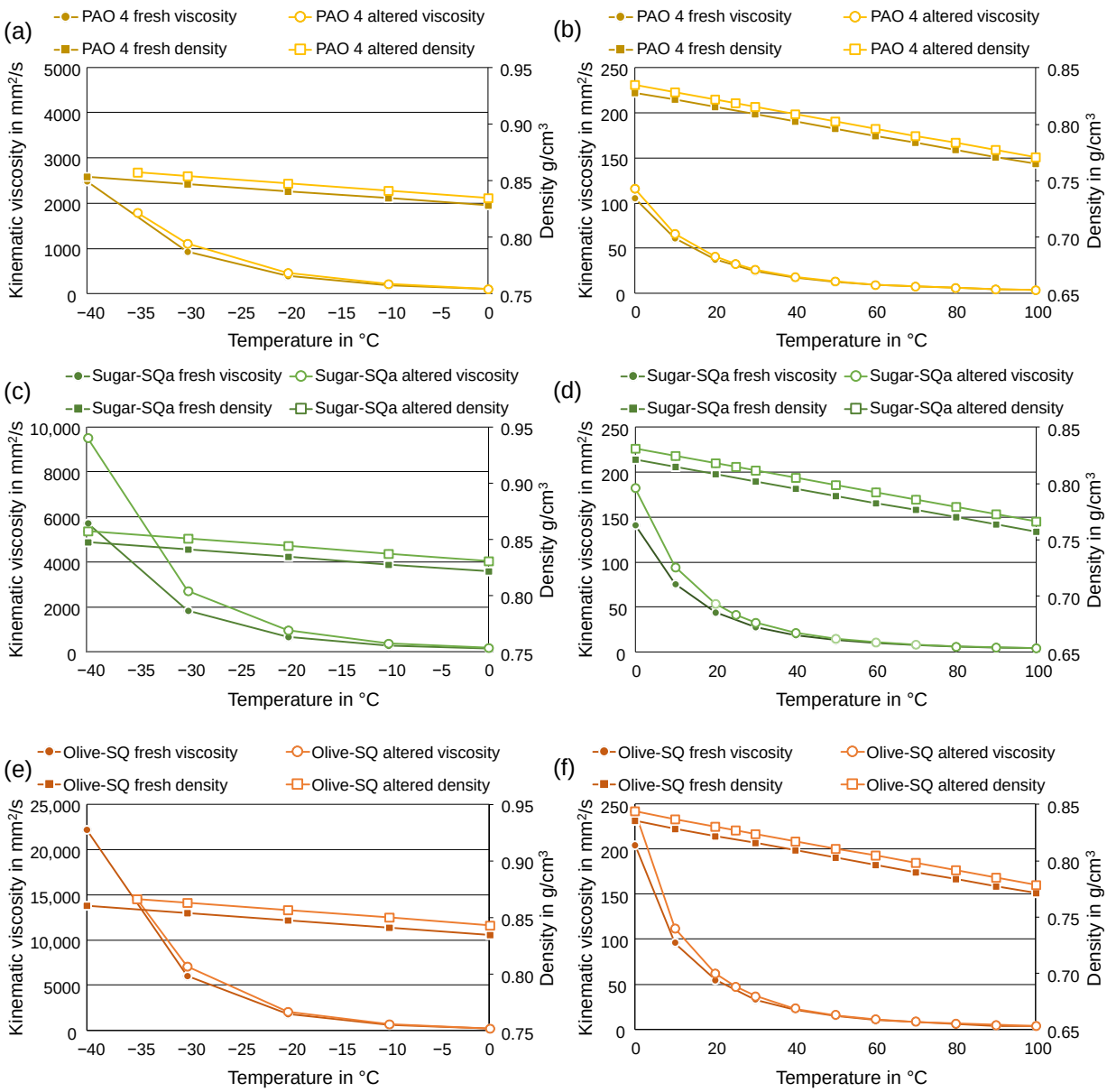

Figure 5. Comparison of the kinematic viscosity and density of the fresh and final altered oil samples. (**a**) PAO 4, low temperature range, (**b**) PAO 4, high temperature range, (**c**) Sugar-SQa, low temperature range, (**d**) Sugar-SQa, high temperature range, (**e**) Olive-SQ, low temperature range, (**f**) Olive-SQ, high temperature range.

Sugar-SQa in Figure 5c,d exhibits elevated viscosity and density after artificial alteration. The differences in viscosity to the fresh oil sample are mostly present in the temperature range below −30 °C but also measurable up to +30 °C. The high-temperature viscosity is largely similar. Comparatively, the density shows a constant offset, which is not dependent on the temperature.

Olive-SQ in Figure 5e,f shows some increase in viscosity or density due to artificial alteration. It was also not possible to accurately measure the viscosity of the final altered oil sample at −40 °C. Overall, kinematic viscosity shows pronounced deviations between fresh and altered oil samples at temperatures below 30 °C.

To provide quantitative numbers for and to identify changes of the viscosity–temperature behavior of fresh and final altered oil samples, the Ubbelohde–Walther equation was applied to the viscometric data [54,55]:

$$\log_{10}(\log_{10}(Z)) = A - B \log_{10} T \quad (1)$$

$$Z = \nu + 0.7 + 10^{(-1.47-1.84\nu-0.51\nu^2)} \quad (2)$$

where ν is the kinematic viscosity in (mm^2/s) and T is the temperature in (K), and A and B are empirical factors of the linear trend obtained. While the offset A stands for the global viscosity level of an oil, the gradient B describes the viscosity–temperature behavior. Table 4 summarizes the results for A and B. All linear fits show a coefficient of determination R^2 of 0.9990 or better. In general, fresh and respective final altered samples are comparable to each other but show some changes due to oxidation, as expected: Higher values of A refer to an increase in viscosity, while lower values of B point to a more distinctive viscosity–temperature behavior. The squalane oil samples, especially the Olive-SQ, show a higher dependence of viscosity from temperature compared to PAO 4.

Table 4. A and B calculated from Ubbelohde–Walther equation for fresh and altered base oils.

Oil Sample	Fresh		Final Altered	
	A	***B***	***A***	***B***
PAO 4	8.75	−3.47	8.89	−3.52
Sugar-SQa	9.23	−3.65	9.42	−3.72
Olive-SQ	9.87	−3.90	9.98	−3.94

3.3. GC Characterization of Fresh and Altered Base-Oil Samples

3.3.1. Simulated Distillation

Simulated distillation via GC-FID revealed the boiling-range distribution of the selected base-oil samples (see Table 5 and Figure 4). The main fraction is detected in the range from 425 to 450 °C, characterized by a steep increase in weight fraction. In the fresh condition, the main fraction is smallest for PAO 4 (35 wt%), followed by Olive-SQ (43 wt%) and Sugar-SQa (54 wt%). PAO 4 shows a fraction of about 19 wt% at lower molecular weight (MW) and 46 wt% at higher MW (related to the C40 distillation fraction [56]). The low-MW fractions of the squalane base oils range from 19 to 25 wt%; higher-MW compounds sum up from 27 to 32 wt% for these samples.

Table 5. Boiling behavior of fresh and altered base oils determined by simulated distillation.

Oil Sample	Starting Point (°C)	End Point (°C)	Low-MW Fraction (wt%)	Main Fraction (wt%)	High-MW Fraction (wt%)
PAO 4 fresh	330	594	19	35	46
PAO 4 altered	333	576	20	30	50
Sugar-SQa fresh	344	538	19	54	27
Sugar-SQa altered	335	510	18	63	19
Olive-SQ fresh	306	556	25	43	32
Olive-SQ altered	317	508	19	59	22

During the artificial alteration of PAO 4, no pronounced change in the distillation starting point (330 vs. 333 °C) is noticed. Also, the low-MW fraction remains constant regardless of the compounds that disappeared or formed during alteration. A lower end point is detected (594 vs. 576 °C) pointing to the removal of high-boiling compounds

during the oxidation process. However, the high-MW fraction (46 vs. 50 wt%) is increased at the expense of the main fraction (35 vs. 30 wt%).

The oxidation behavior of the squalane base oils differs significantly from PAO 4. While the starting points of the distillation curves do not show a clear trend, the end point is significantly reduced after artificial alteration by 28 °C for Sugar-SQa and 48 °C for Olive-SQ, respectively. The low- and high-MW fractions are decreased by 1 to 10 wt%. In turn, the main fractions are significantly increased by 9 and 16 wt%.

It is noted that a direct comparison of results from simulated distillation by GC-FID with findings from GC-MS (next chapter) is not possible for several reasons: Base-oil samples for simulated distillation were directly diluted in solvent without prior preparation, signal intensity is related to the amount of carbon. For GC-MS and structure identification, the oil samples were silylated to capture carboxylic acids and alcohols. Peak intensities heavily depend on the ionization properties of the individual compounds and hence do not clearly indicate quantitative abundances without calibration.

3.3.2. GC-MS and Identification of Degradation Products

As shown in Figure 6 for all base oils, some changes in the original $C_{30}H_{62}$ hydrocarbon peak (RT = 22–27 min) could be detected after 8.6, 8.5, and 38 h of alteration duration for PAO 4, Sugar-SQa and Olive-SQ, most pronounced for Sugar-SQa. Detailed GC-MS analyses of fresh, intermediate and final altered oil samples are displayed in Figures S5–S8. The C30 peak, dominant in all samples, might mask other components or degradation products (e.g., ones with higher unsaturation) due to its broad peak width and intensity. As already indicated by data from simulated distillation, peaks are visible for PAO 4 at higher retention-time ranges corresponding to higher MW compounds related to the C40 distillation fraction [56]. For all base oils, peaks appear in the lower retention-time ranges (lower-MW compounds), most pronounced for Olive-SQ. The chromatograms of fresh Sugar-SQa and Olive-SQ underpin differences in purity, the effects of which have already been revealed in different physicochemical properties and degradation behaviors.

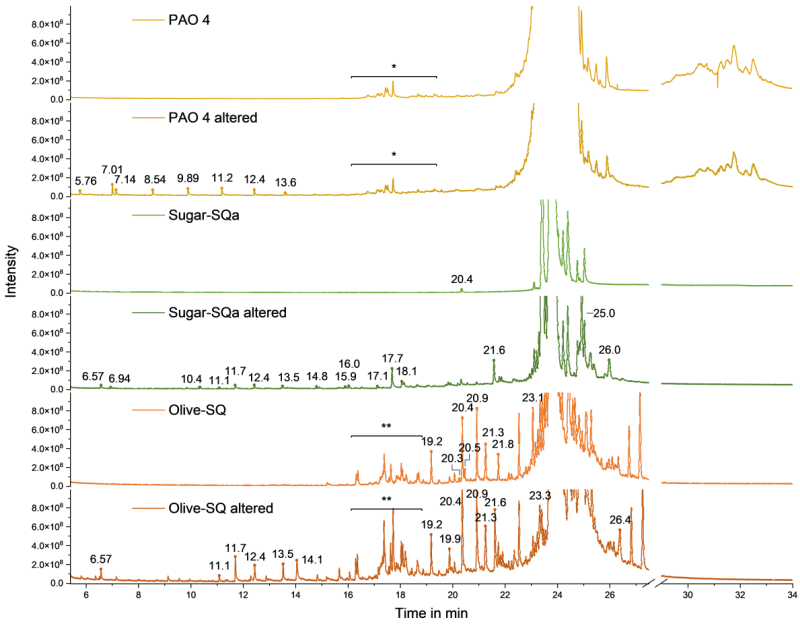

Figure 6. GC-MS chromatogram zoom of components found in fresh and final altered oils, displayed in relative intensities. Peaks changing throughout artificial alteration of base oils are highlighted with their retention times. The compound peaks labeled with retention times and found within the ranges of * and ** are described in Table 6.

Table 6. GC-MS compounds identified in fresh and altered base oils based on evaluation using NIST mass spectral library. Compounds only abundant in fresh PAO 4 are marked with $^{+}$, these in Sugar-SQa $^{++}$, and those in Olive-SQ with $^{+++}$. * and ** refer to the labeled compound peaks in Figure 6.

Type	Retention Time in min	Substance
PAO 4	5.76	Pentanoic acid (C5), TMS
	7.01	Derivatization agent
	7.14	Hexanoic acid (C6), TMS
	8.54	Heptanoic acid (C7), TMS
	9.89	Octanoic acid (C8), TMS
	11.2	Nonanoic acid (C9), TMS
	12.4	Decanoic acid (C10), TMS
	13.6	Undecanoic acid (C11), TMS
	* $^{+}$	Alkanes
Squalanes	6.57	4-Methylvaleric acid (C6), TMS
	6.94	Derivatization agent
	10.4	Alcohol compound
	11.1	3,7-Dimethyloctanoic acid (C10), TMS
	11.7	6,10-Dimethyl-2-undecanone (C13)
	12.4	7-Methyldecanoic acid (C11), TMS
	13.5	Alkane
	14.1	Alkane
	14.8	2-Methylundecanoic acid (C12), TMS
	15.9	Alcohol compound
	16.0	n-Pentadecanoic acid (C15), TMS
	** $^{+++}$	Alcohols/esters/hydrocarbons
	17.1	Hexadecanoic acid (C16), TMS
	17.7	Ketone compound (C18)
	18.1	Heptadecanoic acid (C17), TMS
	19.2 $^{+++}$	Alkane
	19.9	Alkane
	20.3 $^{+++}$	Octadecenoic acid (C18), TMS
	20.4 $^{++}$	Alkane
	20.5 $^{+++}$	Octadecanoic acid (C18), TMS
	20.9 $^{+++}$	Alkane
	21.3 $^{+++}$	Alkene
	21.6	Ketone compound
	21.8 $^{+++}$	Alkane
	23.1–24.1	Squalane
	25.0	Alkene
	26.0	Unidentified
	26.4	Unidentified

The chromatograms of PAO 4 and squalanes show that the degradation products found in the final oil samples are different. In detail, the oxidation of PAO 4 results in shorter-chain degradation products, whereas the oxidative degradation of the squalanes leads to longer-chain degradation products. PAO 4 and Sugar-SQa have comparable thermo-oxidative stability, characterized by the formation of smaller amounts of degradation products. The extraordinary oxidation stability of Olive-SQ compared to Sugar-SQa is attributed to its impurities found beside the main component, $C_{30}H_{62}$.

In Table 6, newly formed or significantly changing peaks are provided with their corresponding retention times and were identified by NIST mass spectral library. For the squalane base oils, branched monocarboxylic acids with the given number of carbon atoms can be expected instead of the proposed NIST assignments that target mostly linear structures. The buildup or decrease in components in intermediate samples through-

out thermo-oxidative alteration is shown in Figures S6–S8 for PAO 4, Sugar-SQa and Olive-SQ, respectively.

As already shown in Figure 6, the main degradation products of PAO 4 are carboxylic acids with short to medium chain lengths, whereas carboxylic acids with medium to long chain lengths (supported by [36]), ketones, and alcohols (also confirmed by FT-IR) were primarily found as degradation products of Sugar-SQa and Olive-SQ due to the structural differences related to more tertiary carbon atoms and methyl groups. Especially C5 to C11 monocarboxylic acids formed during the degradation of PAO 4. The degradation of squalane resulted in the formation of C6, C10 to C12, and C15 to C18 monocarboxylic acids. Ketones and a significant peak of an unsaturated $C_{35}H_{70}$ hydrocarbon (retention time of 25.0 min, Figure S5) are also more pronounced degradation products in Olive-SQ than Sugar-SQa. Compared to PAO 4, the squalane base oils show a tendency towards dehydrogenation and hence an increase in unsaturation as part of their degradation pathway (see alkenes in Table 6 and Section 3.4).

3.4. High-Resolution Mass Spectrometry

Figure 7 shows the identified heteroatom-containing hydrocarbon structures in the fresh base-oil samples in ESI negative-ion mode. Most notably, the Olive-SQ sample contains an amidic structure that is not present in the other two base oils, namely m/z 372.304, being a chloride adduct due to the solvent applied. Besides this organic amide, monoglycerides (MGs) are present in Olive-SQ, which are composed of glycerol and palmitic acid (C16:0, m/z 365.246) or stearic acid (C18:0, m/z 393.277), also detected in the form of chloride adducts. The amide can be attributed to the raw material of the Olive-SQ, which consists of olive waste, and as amides are generally found in olives [57]. It is generally expected that MGs are present since they are also components of olive oil. All these compounds are completely depleted during artificial alteration, see Figure S9. The amidic compound and its consumption during artificial alteration might be responsible for the elevated oxidation stability of the Olive-SQ sample compared to the other base oils, as several amidic compounds are known to scavenge free radicals and thus exhibit antioxidative activity [57]. The impurities in Olive-SQ most probably lead to the high pour point, which makes it less suitable for applications with temperatures below 0 °C.

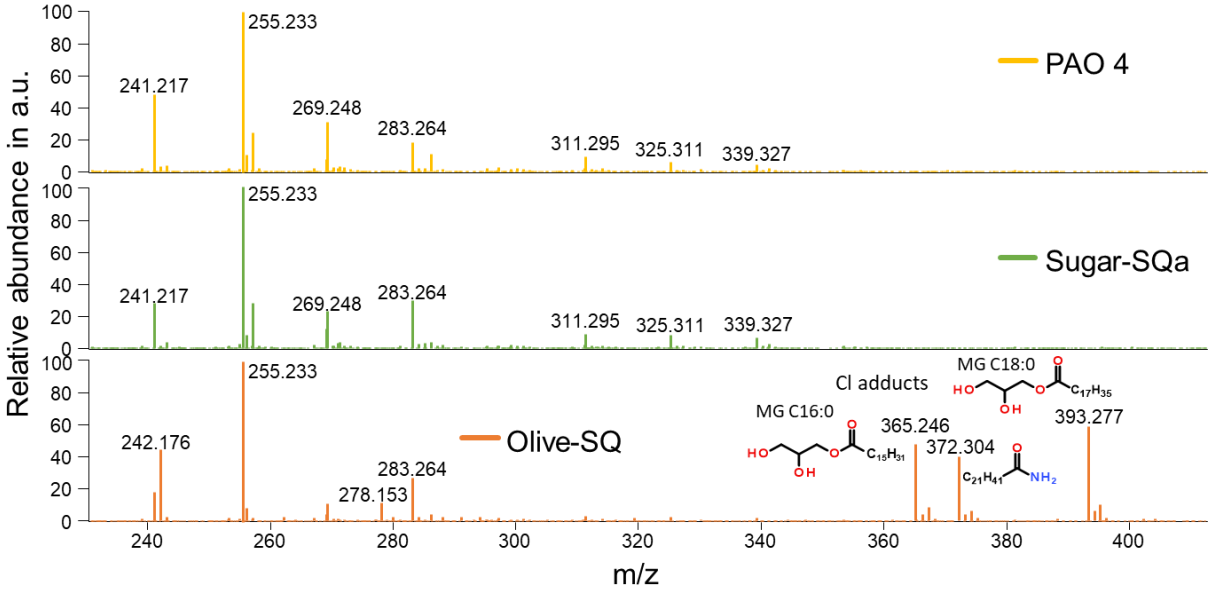

Figure 7. Abundance of organic amide and monoglycerides (MGs) in fresh base oils at comparable intensities. TIC mass spectra in ESI negative-ion mode.

Figure 8 depicts TIC mass spectra acquired in ESI positive-ion mode and offers an overview of the identified dehydrogenization products in the fresh and final oil samples. Dehydrogenation products refer to oxidized and non-oxidized hydrocarbon structures with unsaturated bonds. Dehydrogenation products are largely absent from all fresh base oils. Comparatively, both final altered squalanes contain a high number of dehydrogenation products with higher abundance, which are mostly absent in the final altered PAO 4. These findings correspond well with the FT-IR results in Figure 4e, where a larger amount of unsaturated hydrocarbon moieties in the squalane samples was already highlighted.

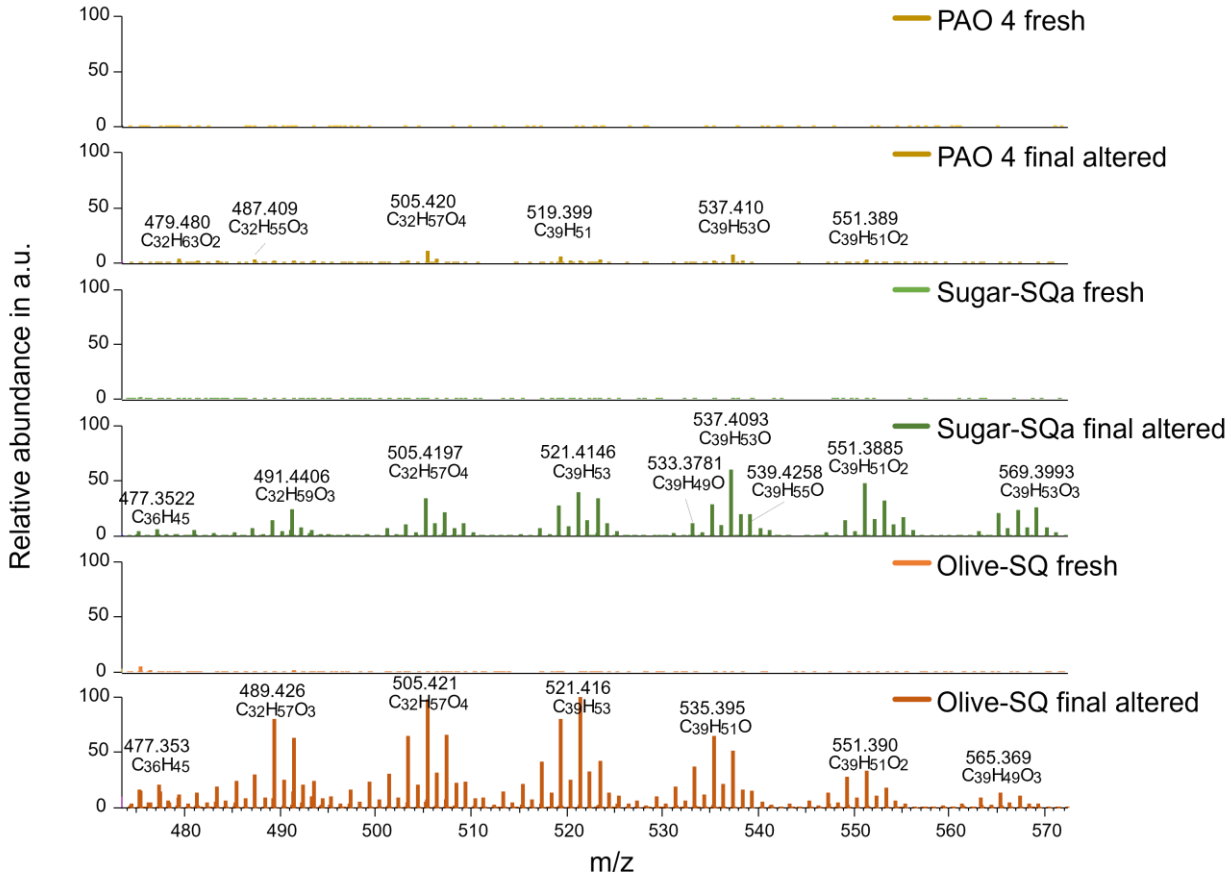

Figure 8. Dehydrogenation products identified in the final altered oil samples at comparable intensities. TIC mass spectra in ESI positive-ion mode.

3.5. Summary

As with the fresh base oils, PAO 4 and Sugar-SQa showed comparable pour points of −75 °C and −72 °C, respectively, despite the differences in the chemical structures of the three isomeric $C_{30}H_{62}$ base oils (Table 3). While kinematic viscosity at 100 °C also provided comparable values of 4.0 and 4.1 mm^2/s, Sugar-SQa is characterized by higher viscosities at temperatures underneath. Olive-SQ, however, exhibited a significantly higher pour point and viscosities compared to the other base oils, up to a factor of 4.4 with respect to PAO 4 at −20 °C. Such deviating properties can be attributed to the presence of impurities with a long and straight chain. In fact, HR-MS revealed an organic amide and monoglycerides as impurities in Olive-SQ, which were not detected in Sugar-SQa and PAO 4 (Figure 7).

Neat squalane and PAO base oils were then oxidatively altered at an elevated temperature of 120 °C until the maximum oxygen consumption was reached. Intermediate oil samples were taken regularly in intervals of 1 h to determine the thermo-oxidative degradation process. The intermediate and final oil samples were subjected to conventional analyses, including viscosity, density, water content, neutralization number, oxidation,

unsaturation, and boiling-range distribution. Furthermore, advanced chemical analyses applying GC-MS and HR-MS provided insights into the chemical structures of the evolved degradation products. These findings were used to build relationships with the property changes of the conventional oil parameters and correlate the results of thermo-oxidative stability to differences in the base-oil composition.

Table 7 provides a qualitative evaluation of all properties and their changes due to oxidation found in this study. PAO 4 and Sugar-SQa are comparable with regard to oxidation induction time and total oxidation time, while these properties are significantly extended by Olive-SQa (Figures 3 and 4). Since impurities were identified as the main difference between Sugar-SQa and Olive-SQ, these are considered to be the cause for the different oxidation stability of the two squalanes. For this reason, further evaluation was carried out comparing PAO 4 with the "clean" Sugar-SQa. The different chemical structures led to a pronounced formation of oxidation products with PAO 4, whereas a comparatively greater tendency to unsaturation and water formation was found with Sugar-SQa. Consequently, trends of oxidation and neutralization correlate as well as those of unsaturation and water content (Figure 4). These findings suggest that squalanes are more susceptible to degradation reactions leading to unsaturation than PAOs (Figure 8). As expected, the formation of degradation products results in increased viscosity and a higher dependence of viscosity from temperature, which was more pronounced for Sugar-SQa (Table 4). The different oxidation behavior is also reflected in the boiling-range distribution, where inverse changes in the proportions in the main fraction and high-MW fraction were observed (Table 5). In the case of Sugar-SQa (and Olive-SQ), this seems to occur such that components in the high-MW fraction are depleted, and degradation products are increasingly found in the main fraction.

Table 7. Property changes due to oxidation of PAO 4, Sugar-SQa and Olive-SQ.

Property	PAO 4	Sugar-SQa	Olive-SQ
Oxidation induction time	+	+	++
Total oxidation time	+	+	+++
Oxidation	++	+	++
Unsaturation	+	++	++
Neutralization number	++	+	++
Water content	+	+++	+++
Viscosity–temperature behavior *A*	+	++	+
Viscosity–temperature behavior *B*	−	−−	−
Simulated distillation starting point	+	−−	++
Simulated distillation end point	−−	−−−	−−−
Simulated distillation low-MW fraction	+	−	−−
Simulated distillation main fraction	−	++	+++
Simulated distillation high-MW fraction	+	−−	−−
Main degradation products	Acids with short/medium chain length	Acids with medium/long chain length, ketones, alcohols	Acids with medium/long chain length, ketones, alcohols
Heteroatom-containing hydrocarbons	None detected	None detected	Amide, monoglycerides
Dehydrogenation products	+	++	+++

−−−/+++ strongly decreasing/increasing, −−/++ decreasing/increasing, −/+ slightly decreasing/slightly increasing.

Conventional and advanced analyses via GC-MS and HR-MS revealed that the major degradation products of PAO 4 were carboxylic acids with short to medium chain lengths, whereas squalane base oils formed more ketones, alcohols, water, and carboxylic acids with medium to long chain lengths (Figure 6, Table 6). These differences result from structural

variations of $C_{30}H_{62}$ base oils, i.e., the number of methyl groups (four in PAO 4 vs. eight in squalanes) and tertiary carbons (two in PAO 4 vs. six in squalanes), rather than product origin and impurities (Figure 1, Table 1). The predominant presence of carboxylic acids in PAO 4 indicates a more advanced hydrocarbon degradation than the ketones and water in squalane base oils.

The (aut)oxidation of hydrocarbons such as lubricant base oils is a complex process driven by free radical reactions, i.e., by homolysis. There is an extensive literature describing the oxidation steps from initiation via the chain propagation and multiplication of free radicals to termination, as well as the effect of antioxidants, e.g., [58,59].

The oxidation process was examined on the basis of several degradation products, especially where the identification of the chemical structures can be assumed to be certain. In this consideration, only tertiary carbon atoms are taken into account, as these tend to form carbon-centered radicals (alkyl radicals) through dissociation of the C-H bond [52]. A free radical is initially formed by eliminating a hydrogen atom (H•) from a labile C-H bond and leaving an alkyl radical (R•). The alkyl radical then couples with an oxygen molecule to form a peroxy radical (ROO•), which in turn abstracts hydrogen from hydrocarbon chains to give a hydroperoxide (ROOH) and generate a new alkyl radical. Hydroperoxides further split into alkoxy (RO•) and hydroxyl (•OH) radicals. Alkoxy and hydroxyl radicals may form new alkyl radicals by abstracting hydrogen atoms from hydrocarbons or give alcohols (ROH) and water (H_2O). Most importantly in this consideration is that oxidation at tertiary carbon atoms leads to alcohols and ketones, but further oxidation causes chain scission between the bond of the tertiary carbon and one of the three neighboring carbons. Based on this assumption, the carboxylic acids formed by the oxidation of PAO 4 are those with a chain length of C8, C10 and C11. Shorter chains appear to be formed by (further) oxidative attack along the hydrocarbon chain. In the same way, the formation of ketones and carboxylic acids from the oxidation of squalanes can be understood: 4-Methylvaleric acid (C6) is an oxidized fragment that is formed by breaking the bond between carbon number 5 (secondary) and 6 (tertiary). Then, 6,10-Dimethyl-2-undecanone (C13) can be formed in a similar way from a chain break between carbon number 10 (tertiary) and 11 (secondary). For a deeper understanding of the oxidation reaction pathways in PAO 4 and squalanes, however, further research is required [35].

As to the possible antioxidative activity of organic amides, Son and Lewis concluded from their studies on synthetic caffeic acid amide and ester analogues that the radical scavenging activity of these compounds was not only determined by the number of hydroxyl groups or catechol moieties but also by the presence of other hydrogen-donating groups such as an amides and sulfhydryls (-SH) [57]. Despite the detection of such organic amides in Olive-SQ, which is an obvious difference in the composition compared to the other two base oils, it cannot be ruled out that enhanced antioxidative activity is due to other factors.

4. Conclusions

Squalane base oils were evaluated against PAO 4 as a benchmark and demonstrated comparable and even enhanced thermo-oxidative stability, depending on product origin and the presence of impurities. While Sugar-SQa matched the stability of PAO 4, Olive-SQ outperformed it, indicating a prolonged lubricant lifetime, which is related to the presence of beneficial impurities. GC-MS was used to identify alkenes, alcohols, ketones and carboxylic acids, from which initial models of the oxidation reaction pathways in PAO 4 and squalane were developed. However, further work is necessary to gain a deeper understanding of the complex oxidation processes. HR-MS revealed an organic amide in fresh Olive-SQ, which was depleted during artificial alteration. The amide might be responsible for the elevated oxidation stability of Olive-SQ compared to PAO

4 and Sugar-SQa, as the literature suggests that some amides exhibit a high free radical scavenging activity, providing an antioxidant function. However, further systematic studies are required to verify this assumption. The abundance of amides and monoglycerides in Olive-SQ may explain the high pour point, which makes it less suitable for applications with temperatures below 0 °C.

Based on the conducted investigations, it is concluded that the sustainable Sugar-SQa could serve as a one-to-one replacement for crude oil-derived PAO 4 thanks to its matching thermo-oxidative stability and rheological properties, especially in the low-temperature region, compared to Olive-SQ. Olive-SQ could also be utilized as an even more thermo-oxidative stable base oil if the high pour point is counteracted with appropriate lubricant additives during the lubricant formulation process.

Further investigations of rheological (i.e., shear and pressure-viscosity dependency), material compatibility (i.e., corrosion, interaction with elastomers) and tribological base-oil properties (i.e., friction and wear characteristics), among others, are needed along with considerations to establish uniformity of the plant-derived base oil's composition to account for the positive and negative attributes of impurities in squalane base oils.

Supplementary Materials: The following supporting information can be downloaded at: https://www.mdpi.com/article/10.3390/lubricants13020048/s1, Figure S1: FT-IR difference spectra of altered PAO 4; Figure S2: FT-IR difference spectra of altered Sugar-SQa; Figure S3: FT-IR difference spectra of altered Olive-SQ; Figure S4: Boiling point distribution of fresh and final altered oils by simulated distillation; Figure S5: Full GC-MS chromatograms of fresh and final altered base oils; Figure S6: GC-MS chromatograms for the comparison of the buildup of degradation products of fresh and altered PAO 4. The *x*-axis is cut, where no interesting products appear; Figure S7: GC-MS chromatograms for the comparison of the buildup of degradation products of fresh and altered Sugar-SQa. The *x*-axis is cut, where no interesting products appear; Figure S8: GC-MS chromatograms for the comparison of the buildup of degradation products of fresh and altered Olive-SQ. The *x*-axis is cut, where no interesting products appear; Figure S9: Organic amide (m/z 372.304) and monoglycerides (m/z 365.246, m/z 393.277) in the fresh and final altered Olive-SQ samples via HR-MS. Intensities are scaled according to the highest intensity in each individual spectrum.

Author Contributions: Conceptualization, J.P., A.A., L.P., I.M., M.F. and N.D.; data curation, J.P., L.P. and I.M.; investigation, J.P., A.A. and L.P.; visualization, J.P. and A.A.; writing—original draft preparation, J.P. and A.A.; writing—review and editing, J.P., A.A., L.P., I.M., M.F. and N.D.; funding acquisition, M.F. and N.D.; project administration, M.F., L.P. and N.D. All authors have read and agreed to the published version of the manuscript.

Funding: This work was carried out as part of the COMET Centre InTribology (FFG no. 906860), a project of the "Excellence Centre for Tribology" (AC^{2}T research GmbH). InTribology is funded within the COMET—Competence Centres for Excellent Technologies Programme by the federal ministries BMK and BMAW as well as the federal states of Niederösterreich and Vorarlberg based on financial support from the project partners involved. COMET is managed by The Austrian Research Promotion Agency (FFG).

Data Availability Statement: The original contributions presented in the study are included in the article; further inquiries can be directed to the corresponding author.

Acknowledgments: We would like to thank our colleagues from AC^{2}T research GmbH for their consultations and supporting analyses carried out within the scope of the presented work.

Conflicts of Interest: Authors Jessica Pichler, Adam Agocs, Lucia Pisarova, Marcella Frauscher and Nicole Dörr were employed by the company AC^{2}T research GmbH. The remaining author declares that the research was conducted in the absence of any commercial or financial relationships that could be construed as a potential conflict of interest.

References

1. Malik, M.A.I.; Kalam, M.A.; Mujtaba, M.A.; Almomani, F. A review of recent advances in the synthesis of environmentally friendly, sustainable, and nontoxic bio-lubricants: Recommendations for the future implementations. *Environ. Technol. Innov.* **2023**, *32*, 103366. [CrossRef]
2. INEOS Oligomers. Durasyn Polyalphaolefin. Available online: https://www.ineos.com/businesses/ineos-oligomers/products/durasyn-polyalphaolefin-pao/ (accessed on 21 November 2024).
3. Rensselar, J.V. The Bright Future for PAOs. February 2021. Available online: https://www.stle.org/files/TLTArchives/2021/02_February/Cover_Story.aspx (accessed on 21 November 2024).
4. European Parliament; Council of the European Union. Commission Decision (EU) 2018/1702 of 8 November 2018 establishing the EU Ecolabel criteria for lubricants (notified under document C(2018) 7125). *Off. J. Eur. Union* **2018**, *285*, 82–96.
5. INEOS Oligomers. Durasyn® Polyalphaolefins: Summary of Environmental Data. 2009. Available online: https://www.ineos.com/globalassets/ineos-group/businesses/ineos-oligomers/she/durasyn-environmental-summary-202009.pdf (accessed on 21 November 2024).
6. Beran, E. Experience with evaluating biodegradability of lubricating base oils. *Tribol. Int.* **2008**, *41*, 1212–1218. [CrossRef]
7. Infineum Insight. Moving to Even Lower Viscosities. June 2022. Available online: https://www.infineuminsight.com/en-gb/articles/moving-to-even-lower-viscosities/ (accessed on 21 November 2024).
8. Eurol, B.V. Thin, Thinner, Thinnest: The Trend Towards Low-Viscosity Engine Oils. March 2020. Available online: https://www.eurol.com/en/updates/knowledge-articles/thin-thinner-thinnest-the-trend-towards-low-viscosity-engine-oils (accessed on 21 November 2024).
9. WECTOL Oil & Carcare Products. Motoröl nach Viskosität. Available online: https://www.addinol-shop.de/pkw-oel/viskositat.html (accessed on 21 November 2024).
10. Emery Oleochemicals. Base Stocks and Components for Electric Vehicle—Oils and Thermal Fluids. 2024. Available online: https://www.emeryoleo.com/sites/default/files/2024-04/Emery-Oleochemicals-Base-Stocks-Components-Electric-Vehicles.pdf (accessed on 21 November 2024).
11. Veluri, R. Electric Vehicle Lubricants. February 2023. Available online: https://www.tribonet.org/industry-news/electric-vehicle-lubricants/ (accessed on 21 November 2024).
12. INEOS Oligomers. Durasyn® 164—Technical Data Sheet. Available online: https://www.ineos.com/show-document/?grade=Durasyn+164&bu=INEOS+Oligomers&documentType=Technical+Data+Sheet&docLanguage=EN&version=d0d59cc79b3ea2924fb74faf79f6d5dd (accessed on 21 November 2024).
13. Yarkent, Ç.; Oncel, S.S. Recent Progress in Microalgal Squalene Production and Its Cosmetic Application. *Biotechnol. Bioprocess Eng.* **2022**, *27*, 295–305. [CrossRef] [PubMed]
14. *OENORM EN 16807*; Liquid Petroleum Products—Bio-Lubricants—Criteria and Requirements of Bio-Lubricants and Bio-Based Lubricants. Austrian Standards International: Wien, Austria, 2016.
15. Vidal-Abarca Garrido, C.; Kaps, R.; Kofoworola, O.; Wolf, O.; Riera, M.R.; Hidalgo, C.; Fuentes, N.; Escamilla, M.; Janer, G.; Josa, J.; et al. Revision of the European Ecolabel Criteria for Lubricants. 2018. Available online: https://ec.europa.eu/environment/ecolabel/documents/Final%20Report%20EU%20Ecolabel%20Lubricants.pdf (accessed on 4 December 2024).
16. CIRCABC. *Lubricant Substance Classification List (LuSC-List) 01/10/2024*. November 2024. Available online: https://circabc.europa.eu/ui/group/0e3024d9-38be-415b-b141-c05d5d31dd92/library/997552dd-7098-4ffb-87db-3590fc2ff32e/details (accessed on 4 December 2024).
17. European Commission. EU Ecolabel—Lubricants. Available online: https://environment.ec.europa.eu/topics/circular-economy/eu-ecolabel/product-groups-and-criteria/lubricants_en (accessed on 21 November 2024).
18. U.S. Environmental Protection Agency (EPA). Vessel General Permit for Discharges Incidental to the Normal Operation of Vessels (VGP). 2013. Available online: https://www3.epa.gov/npdes/pubs/vgp_permit2013.pdf (accessed on 4 December 2024).
19. Valvoline Global Operations. What Are Environmentally-Friendly Lubricants? Available online: https://www.valvolineglobal.com/en-eur/what-are-environmentally-friendly-lubricants/ (accessed on 21 November 2024).
20. Tenenbaum, D.J. Food vs. Fuel: Diversion of Crops Could Cause More Hunger. *Environ. Health Perspect.* **2008**, *116*, A254–A257. [CrossRef] [PubMed]
21. European Parliament; Council of the European Union. Directive (EU) 2018/2001 of the European Parliament and of the Council of 11 December 2018 on the promotion of the use of energy from renewable sources (recast) (Text with EEA relevance). *Off. J. Eur. Union* **2018**, *328*, 82–209.
22. European Court of Auditors. The EU's Support for Sustainable Biofuels in Transport—An Unclear Route Ahead. 2023. Available online: https://www.eca.europa.eu/ECAPublications/SR-2023-29/SR-2023-29_EN.pdf (accessed on 21 December 2024).
23. Carus, M.; Dammer, L.; Puente, Á.; Raschka, A.; Arend, O. Bio-Based Drop-in, Smart Drop-in and Dedicated Chemicals. 2017. Available online: https://bioplasticsnews.com/wp-content/uploads/2018/08/RoadToBio_Drop-in_paper.pdf (accessed on 21 December 2024).

24. McPhee, D.; Pin, A.; Kizer, L.; Perelman, L. Deriving Renewable—Squalane from Sugarcane. *Cosmet. Toilet. Mag.* **2014**, *129*, 1–6.
25. Squalane: Benefits for Skin and Usage in Cosmetic. SOPHIM. Available online: https://www.sophim.com/en/squalane/ (accessed on 25 December 2024).
26. Havaej, P.; Degroote, J.; Fauconnier, D. Sensitivity of TEHL Simulations to the Use of Different Models for the Constitutive Behaviour of Lubricants. *Lubricants* **2023**, *11*, 151. [CrossRef]
27. Lee, J.H.C.; Poornachary, S.K.; Tee, X.Y.; Guo, L.; Liu, C.K.; Zhang, L.; Sun, T.; Chen, Q.; Zheng, J.; Chow, P.S. Effect of Base Oil Polarity on the Functional Mechanism of a Viscosity Modifier: Unraveling the Conundrum of Coil Expansion Model. *Ind. Eng. Chem. Res.* **2023**, *62*, 20567–20578. [CrossRef]
28. Schmitt, S.; Fleckenstein, F.; Hasse, H.; Stephan, S. Comparison of Force Fields for the Prediction of Thermophysical Properties of Long Linear and Branched Alkanes. *J. Phys. Chem. B* **2023**, *127*, 1789–1802. [CrossRef]
29. Liu, H.C.; Zhang, B.B.; Bader, N.; Venner, C.H.; Poll, G. Scale and contact geometry effects on friction in thermal EHL: Twin-disc versus ball-on-disc. *Tribol. Int.* **2021**, *154*, 106694. [CrossRef]
30. Liu, H.C.; Zhang, B.B.; Bader, N.; Venner, C.H.; Poll, G. Simplified traction prediction for highly loaded rolling/sliding EHL contacts. *Tribol. Int.* **2020**, *148*, 106335. [CrossRef]
31. Tošić, M.; Larsson, R.; Jovanović, J.; Lohner, T.; Björling, M.; Stahl, K. A Computational Fluid Dynamics Study on Shearing Mechanisms in Thermal Elastohydrodynamic Line Contacts. *Lubricants* **2019**, *7*, 69. [CrossRef]
32. Li, W.; Jadhao, V. Comparing Phenomenological Models of Shear Thinning of Alkanes at Low and High Newtonian Viscosities. *Tribol. Lett.* **2024**, *72*, 112. [CrossRef]
33. *ASTM D943-20*; Standard Test Method for Oxidation Characteristics of Inhibited Mineral Oils. ASTM International: West Conshohocken, PA, USA, 2020. [CrossRef]
34. *ASTM D2272-22*; Standard Test Method for Oxidation Stability of Steam Turbine Oils by Rotating Pressure Vessel. ASTM International: West Conshohocken, PA, USA, 2022. [CrossRef]
35. Frauscher, M.; Besser, C.; Allmaier, G.; Dörr, N. Oxidation Products of Ester-Based Oils with and without Antioxidants Identified by Stable Isotope Labelling and Mass Spectrometry. *Appl. Sci.* **2017**, *7*, 396. [CrossRef]
36. Diaby, M.; Sablier, M.; Le Negrate, A.; El Fassi, M. Kinetic Study of the Thermo-Oxidative Degradation of Squalane (C30H62) Modeling the Base Oil of Engine Lubricants. *J. Eng. Gas Turbines Power* **2009**, *132*, 032805. [CrossRef]
37. Dugmore, T.I.J.; Stark, M.S. Effect of biodiesel on the autoxidation of lubricant base fluids. *Fuel* **2014**, *124*, 91–96. [CrossRef]
38. European Chemicals Agency (ECHA). 2,6,10,15,19,23-hexamethyltetracosane. 2023. Available online: https://echa.europa.eu/de/registration-dossier/-/registered-dossier/14412/5/3/2 (accessed on 4 December 2024).
39. Chevron Phillips Chemical Company LP. Product Stewardship Summary—PAO 4–10 cSt. 2020. Available online: https://www.cpchem.com/sites/default/files/2020-09/PAO%204-10%20PSS%202020%20update%20Rev%202.pdf (accessed on 4 December 2024).
40. Frauscher, M.; Agocs, A.; Besser, C.; Rögner, A.; Allmaier, G.; Dörr, N. Time-Resolved Quantification of Phenolic Antioxidants and Oxidation Products in a Model Fuel by GC-EI-MS/MS. *Energy Fuels* **2020**, *34*, 2674–2682. [CrossRef]
41. *DIN EN 16091*; Liquid Petroleum Products—Middle Distillates and Fatty Acid Methyl Ester (FAME) Fuels and Blends—Determination of Oxidation Stability by Rapid Small Scale Oxidation Test (RSSOT). DIN Deutsches Institut für Normung e. V.: Berlin, Germany, 2022. [CrossRef]
42. *DIN 51453:2024-08*; Testing of Lubricants—Determination of Oxidation and Nitration of Used Motor Oils—Infrared Spectrometric Method. DIN Deutsches Institut für Normung e. V.: Berlin, Germany, 2024.
43. *DIN 51558-2*; Testing of Mineral Oils—Determination of Neutralization Number—Part 2: Color-Indicator Titration, Insulating Oils. DIN Deutsches Institut für Normung e. V.: Berlin, Germany, 2017.
44. *DIN 51777*; Petroleum Products—Determination of Water Content Using Titration According to Karl Fischer. DIN Deutsches Institut für Normung e. V.: Berlin, Germany, 2020. [CrossRef]
45. *ASTM D7042*; Standard Test Method for Dynamic Viscosity and Density of Liquids by Stabinger Viscometer (and the Calculation of Kinematic Viscosity. ASTM International: West Conshohocken, PA, USA, 2021. [CrossRef]
46. *ASTM D2270*; Standard Practice for Calculating Viscosity Index from Kinematic Viscosity at 40 °C and 100 °C. ASTM International: West Conshohocken, PA, USA, 2024. [CrossRef]
47. *DIN EN ISO 3016*; Petroleum and Related Products from Natural or Synthetic Sources—Determination of Pour Point. DIN Deutsches Institut für Normung e. V.: Berlin, Germany, 2019. [CrossRef]
48. *ASTM D6352*; Standard Test Method for Boiling Range Distribution of Petroleum Distillates in Boiling Range from 174 °C to 700 °C by Gas Chromatography. ASTM International: West Conshohocken, PA, USA, 2024. [CrossRef]
49. Pape, P.G. Silylating Agents. In *Kirk-Othmer Encyclopedia of Chemical Technology*; Wiley Online Library: Hoboken, NJ, USA, 2017. [CrossRef]
50. Agocs, A.; Nagy, A.L.; Ristic, A.; Tabakov, Z.M.; Raffai, P.; Besser, C.; Frauscher, M. Oil Degradation Patterns in Diesel and Petrol Engines Observed in the Field—An Approach Applying Mass Spectrometry. *Lubricants* **2023**, *11*, 404. [CrossRef]

51. Frauscher, M. Capillary GC-EI-MS and Low Energy Tandem MS of Base Oils and Additives in Lubricants and Fuels. Ph.D. Thesis, TU Wien, Vienna, Austria, 2019. [CrossRef]
52. Stark, M.S.; Wilkinson, J.J.; Smith, J.R.L.; Alfadhl, A.; Pochopien, B.A. Autoxidation of Branched Alkanes in the Liquid Phase. *Ind. Eng. Chem. Res.* **2011**, *50*, 817–823. [CrossRef]
53. Agocs, A.; Nagy, A.L.; Tabakov, Z.; Perger, J.; Rohde-Brandenburger, J.; Schandl, M.; Besser, C.; Dörr, N. Comprehensive assessment of oil degradation patterns in petrol and diesel engines observed in a field test with passenger cars—Conventional oil analysis and fuel dilution. *Tribol. Int.* **2021**, *161*, 107079. [CrossRef]
54. Seeton, C.J. Viscosity—temperature correlation for liquids. *Tribol. Lett.* **2006**, *22*, 67–78. [CrossRef]
55. *ASTM D341*; Standard Practice for Viscosity—Temperature Equations and Charts for Liquid Petroleum or Hydrocarbon Products. ASTM International: West Conshohocken, PA, USA, 2020. [CrossRef]
56. Wu, M.M.; Ho, S.C.; Forbus, T.R. Synthetic Lubricant Base Stock Processes and Products. In *Practical Advances in Petroleum Processing*; Hsu, C.S., Robinson, P.R., Eds.; Springer: New York, NY, USA, 2006; pp. 553–577. [CrossRef]
57. Son, S.; Lewis, B.A. Free Radical Scavenging and Antioxidative Activity of Caffeic Acid Amide and Ester Analogues: Structure−Activity Relationship. *J. Agric. Food Chem.* **2001**, *50*, 468–472. [CrossRef]
58. Canter, N. Antioxidants—Key additives enable lubricants to operate under more severe conditions. *Tribol. Lubr. Technol.* **2016**, *72*, 10–21.
59. Braun, J. 6.1 Antioxidants. In *Lubricants and Lubrication*, 3rd ed.; Dresel, W., Mang, T., Eds.; Wiley-VCH Verlag GmbH & Co. KGaA: Weinheim, Germany, 2017; pp. 118–123.